

Constructing Compact Brain Connectomes for Individual Fingerprinting

Vikram Ravindra, Petros Drineas, Ananth Grama

Purdue University

Abstract. Recent neuroimaging studies have shown that functional connectomes are unique to individuals, i.e., two distinct fMRIs taken over different sessions of the same subject are more similar in terms of their connectomes than those from two different subjects. In this study, we present significant new results that identify specific parts of the connectome that code the unique signatures. We show that a very small part of the connectome (under 100 features from among over 64K total features) is responsible for the signatures. A network of these features is shown to achieve excellent training and test accuracy in matching imaging datasets. We show that these features are statistically significant, robust to perturbations, invariant across populations, and are localized to a small number of structural regions of the brain (12 regions from among 180). We develop an innovative matrix sampling technique to derive computationally efficient and accurate methods for identifying the discriminating sub-connectome and support all of our claims using state of the art statistical tests and computational techniques.

Keywords: Connectomics, Brain Fingerprinting, Leverage Scores

1 Introduction

The availability of large, high-quality neuro-imaging datasets has motivated important studies of the structure, function, similarity, uniqueness, evolution, and impairment (e.g., neurodegeneracy) of the brain. Consortia such as the Human Connectome Project, 1000 Functional Connectomes Project, and LONI have mapped healthy and diseased brains on a massive scale. These studies have resulted in a rich class of models, methods, and software, along with standardization efforts aimed at cataloging various structural and functional components of the brain.

A large class of functional MRI studies focus on differences between sets of cohorts (e.g., healthy vs. diseased). Such studies characterize an invariant signal within each cohort and identify significant changes in these invariant signals across cohorts. Invariant signals within cohorts are designed to suppress individual level heterogeneity of the functional connectomes, and can be computed using methods that range from simple averaging to sophisticated matching techniques to identify statistically significantly conserved components.

In contrast, a number of recent results have demonstrated that functional connectomes are unique to individuals. Finn et al. [1] show that connectomes constructed from two distinct fMRI sessions of the same subject are more similar than connectomes constructed from two different subjects. Amico et al. [2] show that low-rank approximations provide an excellent basis for characterizing inter-subject variability. In particular, they compute a low-rank approximation of the matrix representing the connectome, and show that this approximation yields excellent discriminating power between individuals in a cohort. None of these methods, though, map discriminating features directly to structural or functional parts of the connectome.

In this work, we significantly build on prior results on uniqueness of individual connectomes by identifying specific parts of the connectome (and their associated structural components – regions of the human cortex) that form discriminating individual signatures. We show that a very small part of the overall connectome is responsible for individual signatures. This discriminating (sub)connectome is associated with as few as 12 brain regions (out of 180 regions annotated in the selected atlas). We demonstrate the statistical significance of this small sample through suitable statistical tests. We show that the sample is robust across cohorts, i.e., the discriminating parts of the connectome are statistically significantly conserved across cohorts, and that it yields excellent training and test accuracy in identifying individuals.

The methodological basis for our results is provided by leverage score sampling of row/column pairs of the matrix representing the connectome. Specifically, row/column pairs are sampled at random with probability drawn from a distribution specified by leverage scores of the matrix. The resulting sampled matrix, also referred to as a sketch, is directly interpretable, and has been shown to have well-defined approximation properties. In this paper, we use a deterministic version of leverage score sampling to construct compact matrix sketches. We demonstrate that these sketches yield excellent accuracy in terms of the discriminating signature, show that these sketches are statistically significant and robust, and are invariant across populations. We map the connectome associated with these sketches to anatomical regions of the brain, and show that a very small fraction of the regions codes much of the discriminating signature.

The rest of the paper is organized as follows: Section 2 describes the state of the art in fingerprinting connectomes, along with alternate approaches based on leverage score sampling. Section 3 presents implementation details, datasets and preprocessing techniques, and key results from the study. Conclusions and avenues for future research are presented in Section 4.

2 Methodology

We analyse functional MRI images by first extracting a functional network from 4D data (three spatial co-ordinates and a temporal co-ordinate). After pre-processing the images, the first step is to divide the brain into smaller regions, also called parcels. There are various parcellation schemes: some rely on explicit

anatomical markers demarcating various regions in a standardized brain (sometimes also called the brain atlas), while others rely on growing an initial set of seeds, and still others rely on connectivity maps (driven by resting state functional MRI and/or diffusion MRI). While there is no consensus on the best way to parcellate the brain, we discuss the rationale behind our choice of a parcellation scheme in Section 3.3. We refer interested readers to Arslan et al. [3] for a more detailed comparison of various parcellation schemes.

Once the brain voxels are mapped into regions, an averaging process reduces the time series from multiple voxels in a region to a single time series that is representative of all voxels in the region. Coherence between the region-wise time series is then computed (this can simply be a dot product of the time series or a correlation coefficient) resulting in a functional network. We compute such functional networks for all subjects, vectorize them, and stack them into a matrix. We describe the construction of this matrix, A , in Section 3.4.

We first discuss the concept of row and column sampling as a general means of feature selection and in particular, leverage score sampling. We then discuss the use of leverage scores to select features for brain fingerprinting.

2.1 Row/column sampling

Given matrix A , an individual entry $a_{i,j}$ corresponds to the weight of the i th edge of subject j . The problem of identifying the most discriminating subset of features then translates to selecting non-zeros from the correlation matrix (row-column pairs) that are most discriminative in terms of individual signatures. In contrast to conventional dimensionality reduction techniques such as Singular Value Decomposition (SVD), the ability to choose rows or columns from a data matrix directly translates to *feature selection*, especially when features have physical meaning. Retaining such features in the matrix sketch can make the underlying physical phenomenon explainable, while also de-noising the data by eliminating non-discriminating features and noise.

Given a matrix $A \in \mathbb{R}^{m \times n}$, one can use the following randomised meta algorithm to create a sketch matrix \tilde{A} that retains s ($< m$) rows.

function ROW_SAMPLE(A, s)

Let \tilde{A} be an empty matrix

for $t = 1$ to s **do**

Randomly sample a row according to the distribution P

Let $A_{i_t, \star}$ be the sampled row, with corresponding probability p_i

Set $\tilde{A}_{t, \star} = \frac{1}{\sqrt{s p_i}} A_{i_t, \star}$

end for

return \tilde{A}

end function

The algorithm samples s rows of A in independent, identically distributed trials according to P s. The rescaling of \tilde{A} ensures that $\tilde{A}^T \tilde{A}$ is unbiased, i.e., $\mathbb{E}[(\tilde{A}^T A)_{i,j}] = (A^T A)_{i,j}, \forall i \in \{1 \dots m\}, j \in \{1 \dots n\}$ [4].

The only unspecified detail is the choice of distribution P . A simple choice is to sample rows uniformly, however, this yields poor results. An intuitively better choice for the distribution relies on the matrix A itself – assigning higher weights to more important elements. A simple non-uniform distribution is based on l_2 sampling, which can be defined as:

$$p_i = \frac{\|A_{i,\star}\|_2^2}{\sum_i \|A_{i,\star}\|_2^2} = \frac{\|A_{i,\star}\|_2^2}{\|A\|_F^2}. \quad (1)$$

Using norm-squared sampling, Drineas et al.[4] prove that:

$$\mathbb{E}[\|A^T A - \tilde{A}^T \tilde{A}\|_F] \leq \frac{1}{\sqrt{s}} \|A\|_F^2. \quad (2)$$

The bounds in Equation 2 imply that \tilde{A} can be used as a proxy for A . However, this approximation introduces an additive error, which depends on $\|A\|_F$. To achieve better bounds, one can make use of the knowledge of column space of A . The associated sampling technique is called leverage score sampling [5].

Leverage Score Sampling. Let $A \in \mathbb{R}^{m \times n}$, with $m \gg n$. Let $U \in \mathbb{R}^{m \times n}$ be any orthonormal matrix spanning the column space of A . Then, $U^T U = I$ and $U U^T = P_A$, which is an m -dimensional projection matrix onto the span of A . Then, probabilities p_i s are defined as:

$$p_i = \frac{\|U_{i,\star}\|_2^2}{\sum_i \|U_{i,\star}\|_2^2} = \frac{1}{n} (P_A)_{i,i} \quad \forall i \in \{1 \dots m\}. \quad (3)$$

The values of p_i s in Equation 3 are known as *statistical leverage scores*.

In our matrix of vectorized edge values, each row contains values expressing functional connectivity markers between the same pair of physical regions on the brain cortex. Hence, leverage scores are indicative of relative importance of edges in discriminating samples. While the randomized approach discussed here helps to understand it better, we find that a deterministic approach performs well in practice. We call this sketching process *Principal Features Subspace Method*.

2.2 Principal Features Subspace Method

As before, let A be the data matrix of connectomes, and U be the orthonormal matrix that spans the column space of A . Additionally, let t be the number of features that need to be retained. An example of such a matrix U is constructed using left singular vectors from a Singular Value Decomposition (SVD) of A . We can then compute the leverage(l) scores of A as:

$$l_i = \|U_{i,\star}\|_2^2, \quad \forall i \in \{1 \dots m\}. \quad (4)$$

We sort the leverage scores and retain the features corresponding to the top t leverage scores. We call this subspace the *principal features subspace*. In contrast

to prior randomized approaches, we select features in a deterministic manner; Cohen et al. [6] provide theoretical bounds for this selection process.

Starting from the matrix of vectorized edge values A , we compute the left singular vectors using SVD. The ordering of edges according to their leverage scores, if robust across different groups, is indicative of a set of features that can accurately fingerprint an individual’s functional connectome. In this case, for a given parcellation scheme, and for a given measure of region-region coherence, we need to apply SVD just once to determine the relevant edges. We present results from our scheme applied to 100 MRI samples to demonstrate powerful new results on the compactness and robustness of the sub-connectome coding individual fingerprints.

2.3 Related Methods

There is significant recent work in characterizing population-level differences from neuroimaging datasets. Given the focus of our work on individual-level differences, we restrict ourselves to significant results in this space, and use them to motivate our new results.

Finn et al. [1] divide the identification task into two steps: whole brain and network specific. In the first step, they perform identification on the basis of the region-wise correlation matrix of the whole brain, and report a success rate of approximately 93%. Following this, they divide the brain into eight functional networks: medial frontal, fronto-parietal, default mode, subcortical-cerebellum, motor, visual I, visual II, and visual association, on the basis of an atlas constructed from the Yale Dataset(268 nodes covering the whole brain). Restricting analysis to each of these regions, they perform the identification task. From this analysis, they find that the networks medial frontal and fronto parietal carry most discriminating features, yielding accuracies as high as 98%. Similar results have also been reported by Miranda-Dominguez et al.[7] and Mueller et al. [8]. However, these results require significant prior knowledge on composite of parcels known to have functional/structural coherence. Our effort takes a similar two-level approach, viewing identification at the whole brain and network levels. Instead of using prior knowledge, we show that the *Principal Features Subspace* yields a comparable identification training accuracy of approximately 96%. Using the features obtained in the training set on the test set, we find that our test accuracy is around 93%, which is significantly higher than that from Finn et al. In contrast to Finn et al. [1], we restrict the analysis in the second step to the regions that are computationally acquired from our first step. The regions obtained from our first step are in fact consistent with those used by Finn et al. in the second step, in that we find regions in the parietal and frontal cortex being over-represented in our top nodes (9 out of 12 belong to fronto-parietal regions). However, the network identified by our method is significantly smaller than the region-specific network of Finn et al. It is shown to be robust, statistically significant, and invariant on test subjects. Restricting ourselves to 24 parcels (which may belong to different networks), we report an accuracy of approximately 96%.

Column/row sampling using randomized techniques have significant benefits, in addition to de-noising and overfitting. Other commonly used de-noising techniques transform the data matrix into a combination of linearly independent (orthogonal) components, using methods such as Principal Component Analysis (PCA) or Singular Value Decomposition (SVD). De-noising can be achieved by discarding the components corresponding to noise, and working with a low rank approximation of the matrix, as explored in context of brain fingerprinting by Amico et al. [2].

Using the “unrelated” subset of HCP subjects, Amico et al. [2] report that using the original data matrix (simply computing correlations with known samples and selecting the most correlated subject for identification) as a fingerprint yielded an accuracy of around 87%. The process of de-noising using low rank approximations yields better results – Amico et al. [2] report an accuracy of 91% for brain fingerprinting resting state fMRIs. As discussed earlier, the advantage of the *principal features subspace* method is that it provides a small set of regions, thereby de-noising data while also making the connectivity matrix much smaller. It also identifies the signature as a set of biologically relevant features.

Finally, we note that we do not consider effects of time, head motion, parcellation schemes, and anatomical differences between subjects in this study. These present excellent opportunities for continuing efforts, in conjunction with our matrix sampling techniques.

3 Results

We now discuss datasets, preprocessing techniques, feature identification, and statistical tests on identified signatures.

3.1 Dataset

The images used in this study are collected as part of the Healthy Young Adult study in the WU-Minn Project [9] by the Human Connectome Project Consortium. The data includes 3T structural and functional MRI for 1113 adults, 7T resting and task magnetoencephalography (MEG) from 184 subjects, and 3T and 7T diffusion data. Full details of the data can be found in vanEssen et al. [10].

The resting state functional MRI is acquired in two sessions (hereafter referred to as S_1 and S_2), which were separated by a few days. The resting state data in each session lasted approximately 30 minutes (15 minutes for L-R and R-L phase encoding). The spatial resolution was $2 \times 2 \times 2 \text{ mm}^3$ and temporal resolution of 720 ms. In this study, we use the L-R encoding from the 100 “unrelated” subjects, which is part of the S900 release. A detailed description of the acquisition protocol is described by Smith et al [11].

3.2 Preprocessing

The preprocessing steps follow the minimum pre-processing pipeline prescribed by Glasser et al. [12] and Smith et al. [11]. The HCP pre-processing steps include spatial pre-processing and temporal pre-processing. We do some additional processing in addition to the standard pipeline.

The goal of spatial pre-processing is to remove spatial artefacts, while leaving useful information intact. It includes correction for spatial distortions due to gradient non-linearity (of magnetic field), followed by correction for head motion of subject during data acquisition, and registration to the structural MRI image. As brains of different subjects are of different sizes, the image is transformed to 2mm MNI co-ordinate system. This is followed by normalizing the 4D image to global mean and masking out non-brain voxels. Finally, the cortical surface vertices and the sub-cortical volumetric vertices are combined into the standard grayordinate space in a CIFTI dense time-series format. The surface cortical voxels are aligned using non-linear surface registration and non-linear volume registration for volume structures, thereby achieving spatial correspondence between images of different subjects. The rationale behind the grayordinate space is explained in Glasser et al. [12]. In this study, we only use time series from cortical vertices.

Temporal pre-processing is particularly important for resting state analyses, as they rely on correlation between voxel time series. These can get corrupted by temporal artefacts that span across several voxels (in contrast, task analyses have pre-determined timed events, which make them robust to temporal artefactual influences). The HCP temporal pre-processing pipeline includes a minimal high pass filter (cutoff of 2000s) and a slow roll off below that point, which achieves a linear de-trending of data. This is followed by ICA (Independent Component Analysis) and FIX (FMRIB’s ICA-based X-Noiseifier). ICA estimates the dimensionality of the data and FIX decomposes fMRI data into a sum of “good” and “bad” components. The “bad” components are then removed from the data. This step is run on volumetric data, as these components don’t respect tissue boundaries. We refer interested readers to Griffanti et al. [13] for a detailed analysis of ICA + FIX.

We follow this by global signal regression – a procedure that regresses out the mean time series out of every voxel. As resting state analyses have shown that fluctuations at low frequencies are due to haemodynamic responses to neural activation, we applied a bandpass filter (0.008Hz to 0.1Hz), as suggested by Amico et al. [2].

3.3 Brain Atlas

The description of a functional connectome as a network requires the identification of a set of nodes and a set of edges between these nodes. A brain atlas defines parcellation schemes that help achieve the first requirement. Ideally, parcels are non-overlapping, locally functionally distinct areas. The variation within a parcel should be dominated by the variation between parcels. While parcellation is

somewhat of an oversimplification, it allows for analyses of a structurally and functionally relevant region \times region network, rather than a raw *voxel* \times *voxel* network.

In our work, the cortical structures are parcellated in accordance with the atlas of Glasser et al. [14]. This atlas consists of 360 regions (180 in each hemisphere), bound by sharp edges on the basis of anatomy, function, and/or topology. Each of the 180 regions are also classified into 22 larger regions, which allows for analysis at a coarser level, if needed. We find that other parcellation schemes either have too few regions, or are annotated on the basis of fewer samples. In contrast, the boundaries in Glasser et al. [14] are drawn using resting state and task fMRI images from 2 groups of 210 subjects, all of which is part of the previously described Human Connectome Project.

3.4 Experimental Setup

The time series data (i.e., a 2D matrix of gray-ordinate *voxel* \times *time-points*) is z-score normalised. Following this, voxels belonging to the same parcel (Section 3.3) are averaged to yield a *region* \times *time-points* matrix. The Pearson Correlation of all pairs of time series is then computed, resulting in a *region* \times *region* correlation matrix. This process is repeated for both sessions S_1 and S_2 of all subjects. Then, the upper triangular matrix of Session S_1 for all subjects is vectorised and stacked next to each other into a *subjects* \times *feature* matrix, where feature is an entry in the correlation matrix. A similar matrix is constructed for Session S_2 as well.

3.5 Experiments and Results

We present and validate a number of important hypotheses relating to the discriminating connectome and discriminating signatures.

H1: A small set of features encode individual signatures. Our first set of experiments is designed to demonstrate our key result, that a small number of features encode signatures that are largely unique to individuals. This is in contrast to prior techniques that do not identify either structural or functional features associated with individual signatures, just that such signatures exist in the aggregate datasets.

To demonstrate this result, the 100 subjects are randomly divided into training set of 80 and test set of 20 samples. The features corresponding to the top 100 leverage scores from Session S_1 of the training set are identified from a total of 64620 potential features using the technique described in Section 3.4. Pair-wise correlation scores are calculated between data points of the two sessions in this restricted features space. The purpose of this experiment is to demonstrate that two Functional Connectomes of the same subject are more similar than two Functional Connectomes belonging to different subjects using only this small feature set. To demonstrate this, we define accuracy as the percentage of

instances where the same individual is matched across the two sessions, S_1 and S_2 . Note that a match is identified as the highest correlation of an individual in S_2 over all individuals in S_1 . For each partition of the dataset into training and test sets, we compute accuracy as defined above. To ensure robustness, we repeat this experiment for 1000 different (random) selections of training and test sets. Table 1 presents accuracy over training and test data, which is very high. To characterize the statistical significance of our feature selection, we repeat the experiment with 100 features chosen at random. The accuracy associated with 100 randomly selected features is much lower – around 55% (Table 2). We also compute an empirical p -value for our selection by selecting 100 features at random and repeating the experiment 10^6 times. None of these instances yielded accuracy values higher than that for our leverage-score based feature selection. This demonstrates high statistical significance of our identified features (p -value: $< 10^{-6}$).

Table 1. Accuracy of leverage score based method for different splits of training and test samples. The results show consistently high training accuracy irrespective of training set size. However, test accuracy goes down as training set size is reduced due to overfitting.

Training/test split	Train Accuracy(%)	Test Accuracy(%)
80/20	96.23 ± 2.24	93.11 ± 3.61
50/50	96.30 ± 2.59	92.94 ± 3.82
30/70	96.81 ± 3.07	90.23 ± 4.30
20/80	97.01 ± 3.22	87.60 ± 5.27
10/90	97.72 ± 2.65	81.86 ± 7.15

H2: The feature set is robust across individuals. Following our first set of experiments that demonstrate that a small number of features code individual signatures, we now show that this feature set is invariant across individuals – namely that the same features are discriminative across different individuals. To demonstrate this, our next experiment uses the same set of features identified using the leverage scores of the training set on the test set. The result of this experiment is presented in Table 2. The high test accuracy indicates that features relevant for the training set are also discriminative for the test set (p -value: $< 10^{-6}$). This suggests an anatomical and/or physiological basis for the features selected.

To further highlight the implication of this result, it is possible to apply a computational procedure to extract features from training and test sets. The computational procedure may be a complex function defined over all features. This is in fact the case with prior methods. In contrast, what our experiment

Table 2. Performance of leverage-score based feature selection technique, compared to a uniformly random selection technique. The significantly higher test and training set accuracies demonstrate the power of leverage score based selection.

Feature Selection Method	Train Accuracy(%)	Test Accuracy(%)
Leverage Score	96.23 ± 2.24	93.11 ± 3.61
Random	54.62 ± 7.76	54.52 ± 7.52

shows is that no such computational procedure is required – rather, a robust selection of sample-invariant features is highly discriminative and accurate.

H3: The size of the discriminating feature set is small. Our first set of experiments demonstrated that a small set of 100 features is robust and statistically significant in its discriminative power. We now seek to determine the smallest such set that can code individual signatures with high accuracy. We design an experiment in which the number of features is iteratively increased (in order of decreasing leverage scores) and the test accuracy is measured in each iteration. The result of this experiment is presented in Figure 1. We note that the test accuracy plateaus at 59 features at 93%. The maximum (95.5%) is achieved using 95 features.

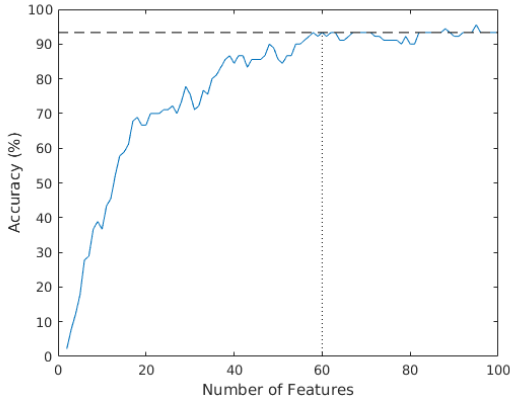


Fig. 1. Variation of test accuracy as a function of feature set size. The rapid convergence in test accuracy demonstrates that a small set of features codes the discriminating signature.

It is important to note that this experiment relies on a leverage score ordering of the features. It is indeed possible that an alternate ordering may yield a smaller

feature set. However, our results on the suitability of leverage scores for feature selection, combined with the rapid plateau of accuracy, strongly suggests that a feature set comprised of 59 to 95 features (from among over 64K features) is enough to code individual signatures with high accuracy.

H4: A small number of structural regions encode the signature. Our previous experiments used entries in the correlation matrix (edges in correlation network) as features. We now investigate whether a small number of structural features (regions in the brain) are capable of coding individual signatures with high discriminating power.

In this experiment, nodes (regions of the brain) participating in the top 60 edges across 1000 iterations are recovered. Their frequencies (the number of edge features a node occurs in) are shown in Figure 2. We construct the sub-network corresponding to the top 12 nodes (regions) thus obtained, and use it to constrain the feature space. The accuracy achieved by this feature set is observed to be 94.05 ± 1.22 across 1000 permutations of 80 subjects. If 12 regions are chosen at random, the mean is 41.47 ± 12.25 (p-value $< 10^{-6}$). This clearly demonstrates that a small number of structural regions code individual signatures with high accuracy. The regions in this set are listed in Table 3.

We can divide the top regions on the basis of structure and function. Structurally, three of the top 12 regions – namely Intra parietal 1, Intra parietal 0, and PF complex belong to the Inferior Parietal Cortex. Furthermore, Lateral Intra Parietal Ventral and Intra Parietal Dorsal belong to the Superior Parietal Complex. Similarly, Area PHT and TE1 Posterior belong to the Lateral Temporal Cortex; and IFJa and Area IFJp belong to the Inferior Frontal Cortex (Supplementary – [14]). This shows that the regions are mostly localised within each lobe (Figure 3).

On the basis of function, we divide parcels into Task Positive and Task Negative Networks. Task Positive Network is a functional network of areas that are activated during tasks that require attention. However, these regions are known to be correlated even during rest. A Task Negative network (also known as a Default Mode Network or DMN) is active when a person is in a state of wakeful rest. It is known to be negatively correlated with Task Positive Networks. Our results show that majority of the top nodes – PHT, PF Complex, IFJa, Temporo-Parieto-Occipital Junction 3, Premotor Eye Field, Intra Parietal 1, Intraparietal Dorsal, IFJp, and Intra Parietal 0 are all implicated in cognitive tasks. The one exception is TE1 Posterior, which is task negative (Supplementary – [14]). This suggests that, even at rest, the signature is coded in the individuals’ cognitive process. As the regions selected are active/inactive over the 7 tasks of the Human Connectome Project, it is possible to use the same set of features, thereby obtaining an activity independent fingerprint.

H5: Our method significantly outperforms state of the art methods in terms of test accuracy. In our final set of experiments, we compare the

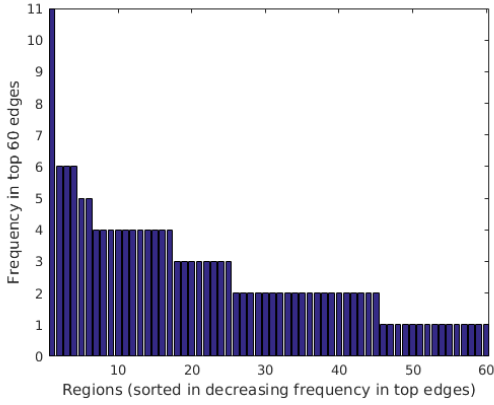


Fig. 2. Frequencies of nodes appearing in the discriminating connectome. The x-axis shows regions (nodes) corresponding to the top edges, and the y-axis shows the frequency of occurrence in the top edges (features). The subnetwork induced by the top 12 regions yields accuracy comparable to that using the entire network.

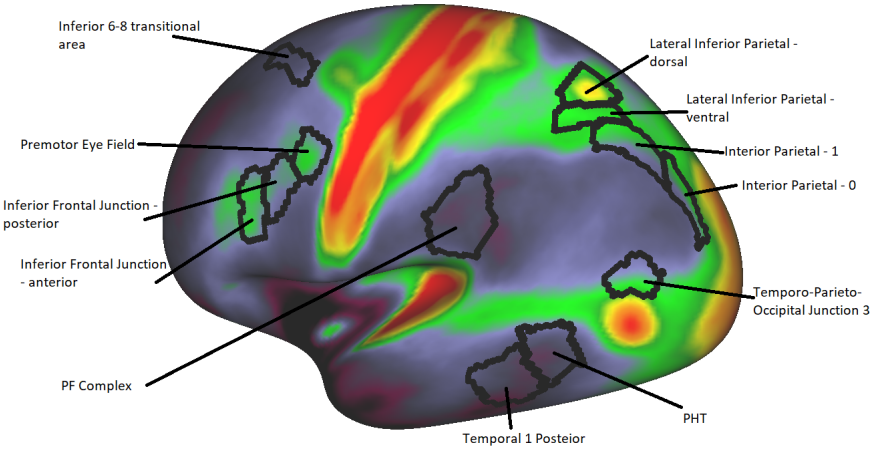


Fig. 3. Lateral view of brain showing top regions that are parts of the discriminating connectome (Parcellation provided by Glasser et al. [14]; visualisation uses the HCP Workbench by Marcus et al. [15]).

Table 3. Top brain regions associated with discriminating features. Legend: O - Occipital, P - Parietal, T - Temporal, F - Frontal, TP - Task Positive, TN - Task Negative, U - unknown.

Area Number	Area Notation	Lobe	Functional Network
137	PHT	O	TP
79	IFJa	O	TP
48	Lateral Intra Parietal Ventral	P	U
141	Temporo-Parieto-Occipital Junction 3	T/P/O	TP
133	TE1 Posterior	T	TN
11	Premotor Eye Field	F	TP
145	Intra Parietal 1	P	TP
97	Inferior 6-8 transitional area	F	U
95	Intraparietal dorsal	P	TP/Dorsal Attention
80	IFJp	F	TP/Cognitive control
148	PF Complex	P	TP
146	Intra Parietal 0	P	TP

accuracy of our method with other state of the art techniques. Finn et al.[1] compute the pairwise Pearson Correlation, with each data point being represented by all elements of the upper diagonal of the time-series correlation matrix. We randomly choose 50 out of 100 subjects and compute pairwise similarity; the accuracy of Finn et al’s method is 88.65 ± 1.76 for this training set. Amico et al. [2], first denoise the data by retaining top singular values. As before, we randomly choose 50 subjects and compute the training set accuracy, shown in Table 4. It is observed that removing the top few singular vectors helps to improve accuracy, since these components correspond to signal that is common to all subjects, as noted by Amico et al.[2]. The test accuracy is computed by removing the top singular components of the train dataset from the test dataset. This reveals that the common signal of the training dataset is an artifact of those particular subjects, and not a pattern that provides significant insights about functional behaviour of the brain. In all cases, our method yields comparable training accuracy, significantly higher test accuracy, while relying on a small set of structurally and functionally interpretable features.

4 Conclusion

We show that the discriminating signature in the human connectome can be defined by the functional activity of a small set of regions limited to the human cerebral cortex. The regions are invariant across individuals. We argued that this definition of a brain signature is better, as it makes the signature interpretable from a biological standpoint, while matching or exceeding the accuracy of previous methods.

Table 4. Comparison of training and test accuracies for various methods. Figures in the first row use the entire matrix, the next five rows use selected singular vectors, and the final row corresponds to our method. The training and test accuracies in the table show that our method achieves close to the best training accuracy and significantly better test accuracy than competing methods.

Principal Components	Train Accuracy(%)	Test Accuracy(%)
All (Same as Finn et al. [1])	88.65 ± 1.76	88.98 ± 1.72
2:end	94.30 ± 1.35	71.76 ± 8.76
11:end	96.74 ± 1.00	69.61 ± 8.94
21:end	95.03 ± 1.90	69.44 ± 8.99
31:end	71.97 ± 6.08	68.95 ± 9.07
41:end	2.77 ± 1.74	65.70 ± 9.59
Principal Features Subspace	96.23 ± 2.24	93.11 ± 3.61

In this study, we limited our validation to resting state functional MRI sessions. It is known that task based functional MRI images present a new set of challenges, since different kinds of task result in activation and de-activation of different parts of the brain. However, the top regions obtained are task positive, which presents the potential to a stronger definition of a signature: one that is invariant across tasks.

References

1. Finn, E.S., Scheinost, D., Finn, D.M., Shen, X., Papademetris, X., Constable, R.T.: Can brain state be manipulated to emphasize individual differences in functional connectivity? *NeuroImage* **160**(1) (2017) 140–151
2. Amico, E., Goni, J.: The quest for identifiability in human functional connectomes. *arXiv:1707.02365* (2017)
3. Arslan, S., Ktena, S.I., Makropoulos, A., Robinson, E.C., Rueckert, D., Parisot, S.: Human brain mapping: A systematic comparison of parcellation methods for the human cerebral cortex. *NeuroImage* (2017)
4. Drineas, P., Kannan, R., Mahoney, M.W.: Fast monte carlo algorithms for matrices I: Approximating matrix multiplication. *SIAM J. Comput.* **36**(1) 132–157
5. Drineas, P., Mahoney, M.W.: Randomnla: Randomized numerical linear algebra. *Communications of the ACM* **59**(6) (2016) 80–90
6. Cohen, M.B., Elder, S., Musco, C., Musco, C., Persu, M.: Dimensionality reduction for k-means clustering and low rank approximation. In: *Proceedings of the Forty-seventh Annual ACM Symposium on Theory of Computing*. STOC '15, New York, NY, USA, ACM (2015) 163–172
7. Miranda-Dominguez, O., Mills, B.D., Carpenter, S.D., Grant, K.A., Kroenke, C.D., Nigg, J.T., Fair, D.A.: Connectotyping: Model based fingerprinting of the functional connectome. *PLOS ONE* **9**(11) (11 2014) 1–16
8. Mueller, S., Wang, D., Fox, M., Yeo, B., Sepulcre, J., Sabuncu, M., Shafee, R., Lu, J., Liu, H.: Individual variability in functional connectivity architecture of the human brain. *Neuron* **77**(3) (2013) 586 – 595

9. Essen, D.C.V., Smith, S.M., Barch, D.M., Behrens, T.E., Yacoub, E., Ugurbil, K.: The wu-minn human connectome project: An overview. *NeuroImage* **80** (2013) 62 – 79
10. Essen, D.V., Ugurbil, K., Auerbach, E., Barch, D., Behrens, T., Bucholz, R., Chang, A., Chen, L., Corbetta, M., Curtiss, S., Penna, S.D., Feinberg, D., Glasser, M., Harel, N., Heath, A., Larson-Prior, L., Marcus, D., Michalareas, G., Moeller, S., Oostenveld, R., Petersen, S., Prior, F., Schlaggar, B., Smith, S., Snyder, A., Xu, J., Yacoub, E.: The human connectome project: A data acquisition perspective. *NeuroImage* **62**(4) (2012) 2222 – 2231
11. Smith, S.M., Beckmann, C.F., Andersson, J., Auerbach, E.J., Bijsterbosch, J., Douaud, G., Duff, E., Feinberg, D.A., Griffanti, L., Harms, M.P., Kelly, M., Laumann, T., Miller, K.L., Moeller, S., Petersen, S., Power, J., Salimi-Khorshidi, G., Snyder, A.Z., Vu, A.T., Woolrich, M.W., Xu, J., Yacoub, E., Ugurbil, K., Essen, D.C.V., Glasser, M.F.: Resting-state fMRI in the human connectome project. *NeuroImage* **80** (2013) 144 – 168
12. Glasser, M.F., Sotiropoulos, S.N., Wilson, J.A., Coalson, T.S., Fischl, B., Andersson, J.L., Xu, J., Jbabdi, S., Webster, M., Polimeni, J.R., Essen, D.C.V., Jenkinson, M.: The minimal preprocessing pipelines for the human connectome project. *NeuroImage* **80** (2013) 105 – 124 Mapping the Connectome.
13. Griffanti, L., Salimi-Khorshidi, G., Beckmann, C.F., Auerbach, E.J., Douaud, G., Sexton, C.E., Zsoldos, E., Ebmeier, K.P., Filippini, N., Mackay, C.E., Moeller, S., Xu, J., Yacoub, E., Baselli, G., Ugurbil, K., Miller, K.L., Smith, S.M.: ICA-based artefact removal and accelerated fMRI acquisition for improved resting state network imaging. *NeuroImage* **95** (2014) 232 – 247
14. Glasser, M.F., Coalson, T.S., Robinson, E.C., Hacker, C.D., Harwell, J., Yacoub, E., Ugurbil, K., Andersson, J., Beckmann, C.F., Jenkinson, M., Smith, S.M., Essen, D.C.V.: A multi-modal parcellation of human cerebral cortex. *Nature* **536** (2016) 171–178
15. Marcus, D., Harwell, J., Olsen, T., Hodge, M., Glasser, M., Prior, F., Jenkinson, M., Laumann, T., Curtiss, S., Van Essen, D.: Informatics and data mining tools and strategies for the human connectome project. *Frontiers in Neuroinformatics* **5** (2011) 4